



Cite this: *Catal. Sci. Technol.*, 2017, 7, 5049

Received 11th August 2017,
Accepted 28th September 2017

DOI: 10.1039/c7cy01637a

rsc.li/catalysis

Computational exploration of ligand effects in copper-catalyzed boracarboxylation of styrene with CO₂†

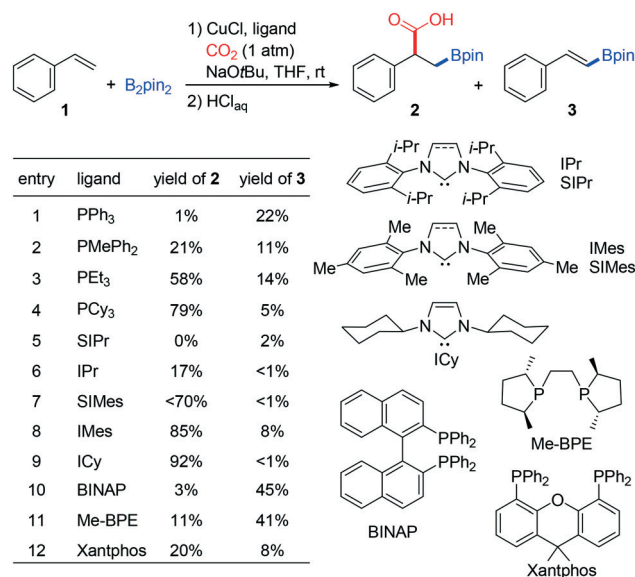
Xiangying Lv,^a Yan-Bo Wu ^b and Gang Lu ^{*c}

The critical ligand effects in copper-catalyzed boracarboxylation of styrene were investigated using density functional theory (DFT) calculations. Based on the rate-determining CO₂ insertion step, the computations reveal that the reactivity of the catalysts ligated by monophosphine ligands is controlled by the ligand's electronic properties. This is consistent with the nature of nucleophilic attack on CO₂ by the benzylcopper intermediate. In contrast, the NHC ligands exert significant steric effects on the reactivity. The ineffectiveness of bidentate phosphine ligands originated from the large distortion of the catalyst and CO₂ that is caused by the sterically congested transition state of CO₂ insertion.

1. Introduction

Olefin carboxylation with CO₂ can not only offer great opportunities for making value-added carboxylic acids,¹ but also motivate the interest in utilizing CO₂ as an appealing C1 building block in organic synthesis.^{2–23} In this connection, various transition metal-based catalytic systems have been developed for accessing the carboxylation of the unsaturated carbon–carbon bond using CO₂.^{24–36} Recently, the Popp group reported a copper-catalyzed boracarboxylation of styrenes with CO₂ and Bpin group into styrene delivers the boracarboxylation product 2 with high regioselectivity (the minor regioisomer is not shown). The undesired borylation product 3 and protoboration product (not shown) can also be obtained under the experimental conditions. The most remarkable feature of this reaction is the significant ligand effect on the reactivity of boracarboxylation. Three types of ligands, monodentate phosphine ligands (*e.g.*, PPh₃, PMePh₂, PEt₃, PCy₃), N-heterocyclic carbene (NHC) ligands (*e.g.*, SIPr, IPr, SIMes, IMes, ICy) and bidentate phosphine ligands (BINAP, Me-BPE,

Xantphos), have been experimentally explored in this reaction. Among these, PCy₃, IMes and ICy supporting copper catalysts are the most active ones (entries 4, 8, and 9). In contrast, other monophosphine and NHC ligands with different P-bound substituents and N-bound substituents display relatively low yields of the desired product 2 (entries 1–3, 5–7). In addition, the bidentate phosphine-based catalysts show quite low reactivities in this reaction (entries 10–12). The origin of these striking ligand effects on reactivity is still unexplored with computations.



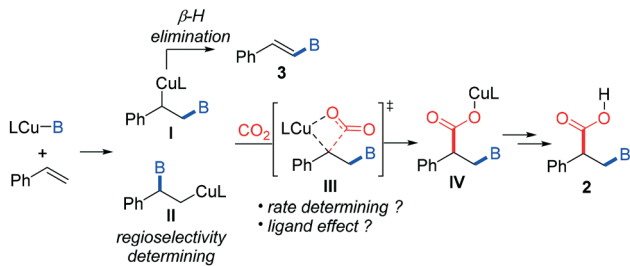
Scheme 1 Cu-catalyzed boracarboxylation of styrene. Experimental conditions: styrene (0.25 mmol), THF (4 mL), B₂pin₂ (1.5 equiv.), NaOtBu (3.0 equiv.), CuCl (12 mol%), phosphine ligand (13 mol%) or (NHC)CuCl (12 mol%).

^a Key Laboratory for Yellow River and Huai River Water Environment and Pollution Control, Ministry of Education, Henan Key Laboratory for Environmental Pollution Control, School of Environment, Henan Normal University, Xinxiang, Henan 453007, P. R. China

^b Key Lab for Materials of Energy Conversion and Storage of Shanxi Province and Key Lab of Chemical Biology and Molecular Engineering of Ministry of Education, Institute of Molecular Science, Shanxi University, Taiyuan, Shanxi, 030006, P. R. China

^c Department of Chemistry, University of Pittsburgh, Pittsburgh, PA, USA.
E-mail: gal40@pitt.edu

† Electronic supplementary information (ESI) available: Additional discussions of computational results; Cartesian coordinates and energies of the optimized structures. See DOI: 10.1039/c7cy01637a



Scheme 2 Proposed mechanism.

The general mechanism of this reaction is straightforward, including the addition of LCu-B to styrene (I and II, Scheme 2), CO_2 insertion into the Cu-C bond (III) and transmetalation with copper carboxylate (IV). The products 2 and 3 are generated from the competing pathways diverged at benzylcopper intermediate I. Although previous studies have gained useful insights into the reaction mechanism,^{38–42} the origin of the ligand effect on the reactivity remains elusive because earlier computational studies often employ small model phosphine and NHC ligands, and do not have a systematic comparison among various different ligands. Herein, we performed DFT calculations to identify how the ligand's electronic and steric properties dominate the reactivity in this copper-catalyzed boracarboxylation reaction.

2. Computational methods

All calculations were performed with Gaussian 09.⁴³ In geometry optimizations, the B3LYP density functional and a mixed basis set of SDD for Cu and 6-31G(d) for other atoms were used. All minima have zero imaginary frequency and all transition states have only one imaginary frequency. Single-point energies were calculated using the M06 functional^{44,45} and a mixed basis set of SDD for Cu and 6-311+G(d,p) for other atoms. Solvation energy corrections were calculated using the SMD model.⁴⁶ THF was used as solvent in the calculations. The same level of theory was often used in recent computational studies of Cu-catalyzed reactions.^{47–49} The natural bond orbital (NBO) charge was calculated at the M06/SDD-6-311+G(d,p) level in the THF solvent based on the geometry optimized at the B3LYP/SDD-6-31G(d) level. The 3D structures of molecules were generated using CYLview.⁵⁰

3. Results and discussion

We first studied the mechanism of Cu-catalyzed boracarboxylation of styrene using CO_2 and B_2pin_2 . LCu-Bpin (4 in Fig. 1), generated from the reaction of LCu-OtBu with B_2pin_2 (see Fig. S1 in the ESI† for details), is considered as the active catalyst. The addition of 4 to styrene determines the regioselectivity of the reaction. The borocupration transition state with Cu attacking the α -carbon of styrene (5-TS, $\Delta G^\ddagger = 11.1$ kcal mol⁻¹) is significantly more favorable than that with Cu attacking the β -carbon of styrene (7-TS, $\Delta G^\ddagger = 22.1$ kcal

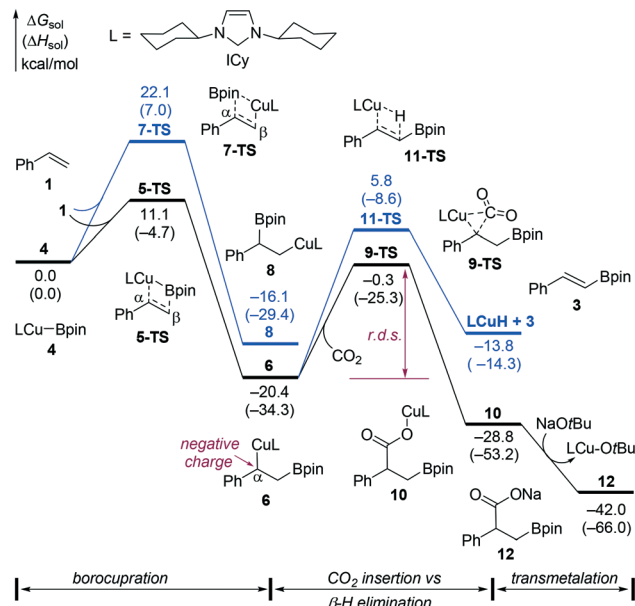


Fig. 1 Energy profile of Cu-catalyzed boracarboxylation of styrene. Energies are with respect to the separated LCu-Bpin and styrene.

mol⁻¹). This is mostly due to the formation of a stable benzylic copper intermediate (6) via 5-TS.³⁸

Two competing pathways, CO_2 insertion and β -H elimination, are possible after the formation of intermediate 6. The β -H elimination pathway is disfavored both kinetically and thermodynamically (11-TS, $\Delta G^\ddagger_{6 \rightarrow 11\text{-TS}} = 26.2$ kcal mol⁻¹). This is in line with the quite low yield of the borylation product 3 when ICy is employed as the ligand (entry 9 in Scheme 1). In contrast, the CO_2 insertion with a barrier of 20.1 kcal mol⁻¹ (9-TS, with respect to 6) is an irreversible process. This represents the rate-determining step in the overall catalytic cycle. The resulting copper carboxylate 10 can be transformed to the major boracarboxylation product 2 via transmetalation and acidification steps.

Based on the rate-determining CO_2 insertion, we then investigated the ligand effect on the reactivity. The computed barriers of CO_2 insertion with different ligands are shown in Table 1. Typically, the nucleophilicity of the negatively charged α -carbon in 6 is crucial for the reactivity of CO_2 insertion.⁵¹ Thus, we calculated the NBO charges on the α -carbon in 6 with different ligands (Table 1). As expected, due to their stronger ability for electron donation, the NHC and bidentate phosphine ligands furnish more negative charges on the α -carbon. However, the trend of the barriers of CO_2 insertion is not consistent with the change of the nucleophilicity of the α -carbon. Although having a more negative charge on the α -carbon, the benzylcopper intermediates with SIPr, IPr and bidentate phosphine ligands lead to higher barriers than those of monophosphine-supported benzylcopper with less negative charges (entries 5, 6, 10–12 vs. entries 1–4). We further plotted the relationship between the barrier of CO_2 insertion and the charge of α -carbon with monophosphine and NHC ligands (Fig. 2). The crossing

Table 1 Ligand effects on the reactivity of CO₂ insertion

Entry	Ligand	Barrier (ΔG^\ddagger , kcal mol ⁻¹)	Charge (<i>e</i>) on α -carbon ^a	$\nu(\text{CO})^b$ (cm ⁻¹)	% V_{bur}
1	PPh ₃	25.5	-0.626	2068.9	26.8
2	PMePh ₂	24.5	-0.629	2067.0	25.1
3	PEt ₃	23.8	-0.635	2061.7	24.8
4	PCy ₃	20.7	-0.635	2056.4	29.0
5	SIPr	27.9	-0.645	2051.5	36.1
6	IPr	26.8	-0.643	2050.5	31.6
7	SIMes	22.7	-0.640	2051.2	32.5
8	IMes	22.7	-0.640	2050.5	31.5
9	ICy	20.1	-0.634	2049.7	26.0
10	BINAP	30.3	-0.655	—	—
11	Me-BPE	27.8	-0.649	—	—
12	Xantphos	26.4	-0.655	—	—

^a The α -carbon of styrene attached to Cu in **6** (Fig. 1). ^b The values taken from ref. 52 and 54.

trend indicates that the reactivity of CO₂ insertion is not only affected by the nucleophilicity of the benzylcopper intermediate. The monophosphine ligand with stronger donicity leads to a lower barrier (*e.g.*, PCy₃). On the contrary, the ICy ligand with the lowest barrier affords the least negative charge compared to other NHC ligands. Therefore, we hypothesize that both the ligand's electronic and steric properties would influence the reactivity of nucleophilic attack on CO₂ by benzylcopper intermediates.

To verify our hypothesis, we use Tolman's electronic parameter (TEP, ν_{CO})⁵² and the buried volume parameter (% V_{bur})⁵³ to study the ligand's electronic and steric effects on the reactivity, respectively. For the monodentate phosphine ligands, a good linear correlation between ΔG^\ddagger and the ligand's TEP (ν_{CO}) was observed ($R^2 = 0.92$, Fig. 3). This indicates that the reactivity of CO₂ insertion with the copper catalyst ligated by monophosphine ligands (*e.g.*, PPh₃, PMePh₂, PEt₃ and PCy₃) is controlled by the ligand's electronic properties. In contrast, ΔG^\ddagger poorly correlates with the TEP of NHC ligands⁵⁴ (see Fig. S2† for details).

Next, we studied the effect of the ligand's steric properties on the reactivity. Unfortunately, for both NHC ligands and monophosphine ligands, we did not observe good correlations between the ΔG^\ddagger of CO₂ insertion and the % V_{bur} ($R^2 = 0.67$ for NHC ligands in Fig. 4; see the correlation with monophosphine ligands in Fig. S3†). Nevertheless, the general

trend shown in Fig. 4 suggests that the reactivity is suppressed by the bulkiness of NHC ligands. The ICy ligand with the smallest % V_{bur} leads to the lowest barrier.

Because the buried volume parameter may oversimplify the catalytic pocket formed by a given ligand,⁵³ certain critical interactions between the catalyst and the substrate may be overlooked. Thus, after finding a general trend of the ligand's steric effect on reactivity shown in Fig. 4, we further compared the optimized geometries of CO₂ insertion transition states with SIPr, IPr, SIMes, IMes and ICy ligands (13-TS-16-TS and 9-TS, Fig. 5a). Clearly, there are repulsive interactions between CO₂ and the NHC ligand in these transition states, as evidenced by the shortest O...H distance (highlighted in red, Fig. 5a). Moreover, the O...H distances in 13-TS/14-TS, 15-TS/16-TS, and 9-TS are significantly different. As can be seen in Fig. 5b, a very good linear correlation between the barrier of CO₂ insertion and the O...H distance between CO₂ and the NHC ligand was observed ($R^2 = 0.97$). This result indicates that the effect of NHC ligands on the reactivity is mostly derived from the steric repulsion between CO₂ and the N-bound substituents. The relatively long O...H distance in 9-TS with the ICy ligand exerts small steric hindrance when incorporating CO₂, thus leading to high reactivity ($\Delta G^\ddagger_{6 \rightarrow 9\text{-TS}} = 20.1$ kcal mol⁻¹). In contrast, because the *ortho*-substituent in the NHC ligand points towards CO₂ in the geometries of transition states (13-TS-16-TS), bulkier

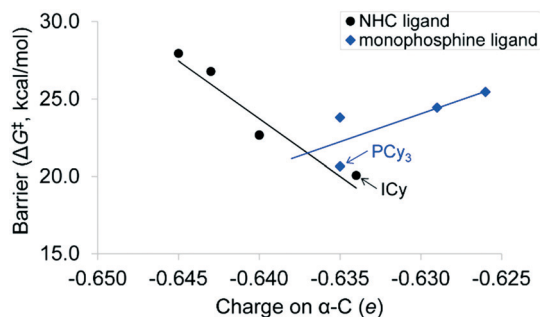


Fig. 2 Relationship between the barrier of CO₂ insertion (ΔG^\ddagger) and the charges on the α -carbon atom.

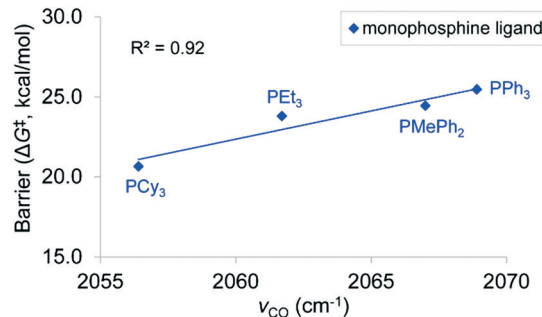


Fig. 3 Correlation between the barrier of CO₂ insertion (ΔG^\ddagger) and the ν_{CO} of monophosphine ligands.

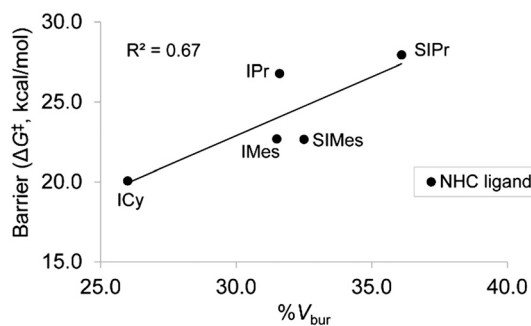


Fig. 4 Correlation between the barrier of CO₂ insertion (ΔG^\ddagger) and the % V_{bur} of NHC ligands.

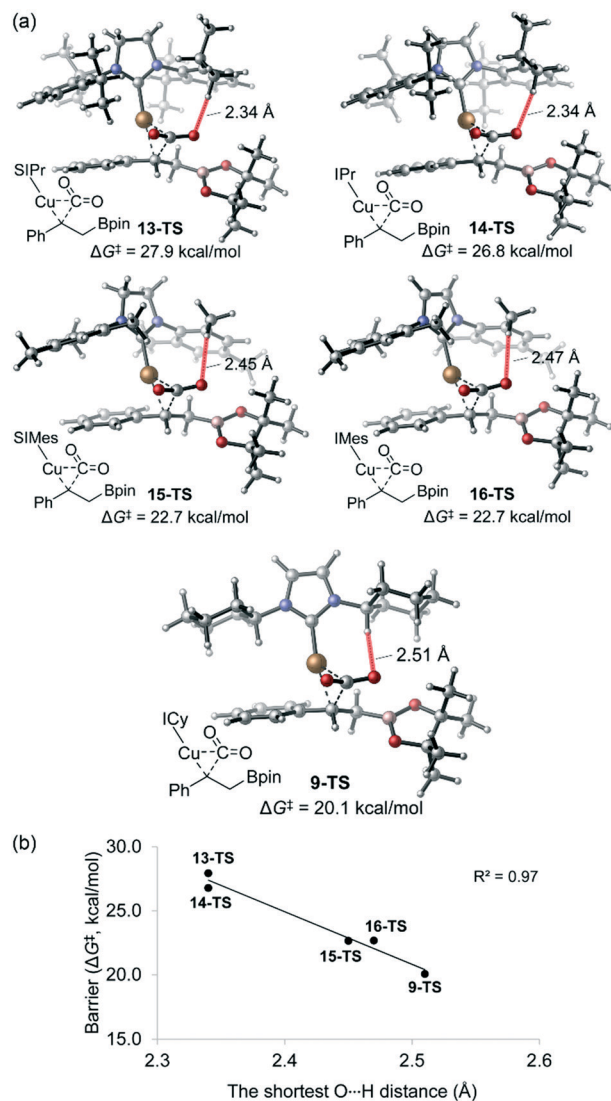


Fig. 5 (a) Optimized geometries of the transition states of CO₂ insertion with different NHC ligands. (b) Correlation between the barrier of CO₂ insertion (ΔG^\ddagger) and the shortest O...H distance between CO₂ and the ligand.

substituents lead to closer proximities to CO₂, resulting in more disfavored repulsions thus decreasing the reactivities (*ortho*-isopropyl substituents in 13-TS/14-TS vs. *ortho*-methyl substituents in 15-TS/16-TS).⁵⁵

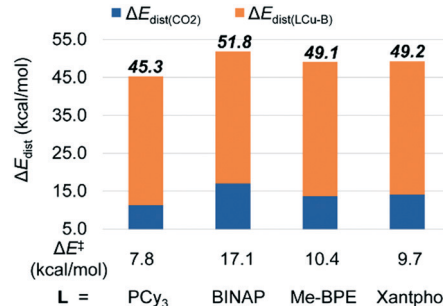


Fig. 6 Computed distortion energies of the CO₂ fragment (shown in blue) and the LCu-Bpin fragment (shown in orange) in the transition states of CO₂ insertion.

Compared to the abovementioned monophosphine ligands and NHC ligands, the catalysts supported by the bidentate phosphine ligands (e.g., BINAP, Me-BPE and Xantphos) show extremely high barriers of CO₂ insertion, although these ligands can dramatically enhance the nucleophilicity of the benzylcopper intermediate (entries 10–12 in Table 1). This can be ascribed to the steric congestion around the four-coordinated copper center in the CO₂ insertion transition states. To better understand the low reactivities with bisphosphine ligands, we used the distortion/interaction model⁵⁶ to analyze the difference in reactivity of the catalysts with PCy₃, BINAP, Me-BPE and Xantphos ligands (Fig. 6). In the distortion/interaction analysis, the geometry of the CO₂ insertion transition state was dissected into two fragments, CO₂ and LCu-Bpin. The distortion energies of each fragment ($\Delta E_{dist}(CO_2)$ and $\Delta E_{dist}(LCu-B)$) from the transition states with bisphosphine ligands are larger than those with PCy₃, respectively. The computed activation energies (ΔE^\ddagger) in the gas phase are consistent with the total distortion energies ($\Delta E_{dist}(CO_2) + \Delta E_{dist}(LCu-B)$) among these four phosphine ligands. This result suggests that the CO₂ insertion is more sensitive to the steric crowdedness of bidentate phosphine ligands than their electronic donorities.

Conclusions

In summary, we performed DFT calculations to investigate the origin of ligand effects in the Cu-catalyzed boracarbonylation of styrene in the presence of B₂pin₂ and CO₂. The computed mechanism indicates that the CO₂ insertion is the rate-determining step in the overall catalytic cycle. Although the nucleophilic attack in the CO₂ insertion step is typically favored by electron-rich benzylcopper intermediates, the computations reveal that both the electronic and steric properties of ligands can affect the reactivity. For monophosphine ligands, the electron donation ability of the ligand is the dominant factor in promoting the reactivity. For NHC ligands and bisphosphine ligands, the bulkiness of the ligand leads to steric repulsions between the ligand and CO₂, or increases the total distortion of the catalyst and CO₂. Both these effects result in low reactivity of CO₂ insertion. These theoretical

insights into ligand effects may be useful for designing efficient transition metal catalysts in CO₂ transformations.

Conflicts of interest

There are no conflicts to declare.

Acknowledgements

This work was supported by the National Natural Science Foundation of China (21507025), the Key Research Project of Henan Province (15A610001), and the Scientific Research Starting Foundation of Henan Normal University (5101219170104).

References

- L. J. Gooßen, N. Rodríguez and K. Gooßen, *Angew. Chem., Int. Ed.*, 2008, **47**, 3100–3120.
- L. Janis, *Curr. Org. Chem.*, 2005, **9**, 605–623.
- T. Sakakura, J.-C. Choi and H. Yasuda, *Chem. Rev.*, 2007, **107**, 2365–2387.
- D. J. Darensbourg, *Chem. Rev.*, 2007, **107**, 2388–2410.
- M. Aresta and A. Dibenedetto, *Dalton Trans.*, 2007, 2975–2992.
- C. M. Rayner, *Org. Process Res. Dev.*, 2007, **11**, 121–132.
- S. N. Riduan and Y. Zhang, *Dalton Trans.*, 2010, **39**, 3347–3357.
- R. Martín and A. W. Kleij, *ChemSusChem*, 2011, **4**, 1259–1263.
- K. Huang, C.-L. Sun and Z.-J. Shi, *Chem. Soc. Rev.*, 2011, **40**, 2435–2452.
- M. Cokoja, C. Bruckmeier, B. Rieger, W. A. Herrmann and F. E. Kühn, *Angew. Chem., Int. Ed.*, 2011, **50**, 8510–8537.
- Y. Tsuji and T. Fujihara, *Chem. Commun.*, 2012, **48**, 9956–9964.
- L. Zhang and Z. Hou, *Chem. Sci.*, 2013, **4**, 3395–3403.
- F. J. Fernandez-Alvarez, A. M. Aitani and L. A. Oro, *Catal. Sci. Technol.*, 2014, **4**, 611–624.
- C. Maeda, Y. Miyazaki and T. Ema, *Catal. Sci. Technol.*, 2014, **4**, 1482–1497.
- C. Martín, G. Fiorani and A. W. Kleij, *ACS Catal.*, 2015, **5**, 1353–1370.
- A. Tlili, E. Blondiaux, X. Frogneux and T. Cantat, *Green Chem.*, 2015, **17**, 157–168.
- B. Yu and L.-N. He, *ChemSusChem*, 2015, **8**, 52–62.
- D. Yu, S. P. Teong and Y. Zhang, *Coord. Chem. Rev.*, 2015, **293**, 279–291.
- S. Wang, G. Du and C. Xi, *Org. Biomol. Chem.*, 2016, **14**, 3666–3676.
- M. Brill, F. Lazreg, C. S. J. Cazin and S. P. Nolan in *Transition metal-catalyzed carboxylation of organic substrates with carbon dioxide*, ed. X. B. Lu, 2016, pp. 225–278.
- M. Ahamed, J. Verbeek, U. Funke, J. Lecina, A. Verbruggen and G. Bormans, *ChemCatChem*, 2016, **8**, 3692–3700.
- M. Börjesson, T. Moragas, D. Gallego and R. Martín, *ACS Catal.*, 2016, **6**, 6739–6749.
- Y. Li, X. Cui, K. Dong, K. Junge and M. Beller, *ACS Catal.*, 2017, **7**, 1077–1086.
- L. Zhang, J. Cheng, B. Carry and Z. Hou, *J. Am. Chem. Soc.*, 2012, **134**, 14314–14317.
- T. Fujihara, Y. Tani, K. Semba, J. Terao and Y. Tsuji, *Angew. Chem., Int. Ed.*, 2012, **51**, 11487–11490.
- Y. Tani, T. Fujihara, J. Terao and Y. Tsuji, *J. Am. Chem. Soc.*, 2014, **136**, 17706–17709.
- B. Miao, S. Li, G. Li and S. Ma, *Org. Lett.*, 2016, **18**, 2556–2559.
- P. Shao, S. Wang, C. Chen and C. Xi, *Org. Lett.*, 2016, **18**, 2050–2053.
- X. Wang, M. Nakajima and R. Martin, *J. Am. Chem. Soc.*, 2015, **137**, 8924–8927.
- T. Fujihara, T. Xu, K. Semba, J. Terao and Y. Tsuji, *Angew. Chem., Int. Ed.*, 2011, **50**, 523–527.
- M. D. Greenhalgh and S. P. Thomas, *J. Am. Chem. Soc.*, 2012, **134**, 11900–11903.
- S. Li, W. Yuan and S. Ma, *Angew. Chem., Int. Ed.*, 2011, **50**, 2578–2582.
- C. M. Williams, J. B. Johnson and T. Rovis, *J. Am. Chem. Soc.*, 2008, **130**, 14936–14937.
- K. Murata, N. Numasawa, K. Shimomaki, J. Takaya and N. Iwasawa, *Chem. Commun.*, 2017, **53**, 3098–3101.
- M. Gaydou, T. Moragas, F. Juliá-Hernández and R. Martín, *J. Am. Chem. Soc.*, 2017, **139**, 12161–12164.
- M. Gaydou, T. Moragas, F. Juliá-Hernández and R. Martín, *J. Am. Chem. Soc.*, 2017, **139**, 12161–12164.
- T. W. Butcher, E. J. McClain, T. G. Hamilton, T. M. Perrone, K. M. Kroner, G. C. Donohoe, N. G. Akhmedov, J. L. Petersen and B. V. Popp, *Org. Lett.*, 2016, **18**, 6428–6431.
- L. Dang, H. Zhao, Z. Lin and T. B. Marder, *Organometallics*, 2007, **26**, 2824–2832.
- H. Zhao, Z. Lin and T. B. Marder, *J. Am. Chem. Soc.*, 2006, **128**, 15637–15643.
- L. Dang, Z. Lin and T. B. Marder, *Organometallics*, 2008, **27**, 4443–4454.
- L. Dang, H. Zhao, Z. Lin and T. B. Marder, *Organometallics*, 2008, **27**, 1178–1186.
- J. Won, D. Noh, J. Yun and J. Y. Lee, *J. Phys. Chem. A*, 2010, **114**, 12112–12115.
- M. J. Frisch, G. W. Trucks, H. B. Schlegel, G. E. Scuseria, M. A. Robb, J. R. Cheeseman, G. Scalmani, V. Barone, B. Mennucci, G. A. Petersson, H. Nakatsuji, M. Caricato, X. Li, H. P. Hratchian, A. F. Izmaylov, J. Bloino, G. Zheng, J. L. Sonnenberg, M. Hada, M. Ehara, K. Toyota, R. Fukuda, J. Hasegawa, M. Ishida, T. Nakajima, Y. Honda, O. Kitao, H. Nakai, T. Vreven, J. A. Montgomery Jr., J. E. Peralta, F. Ogliaro, M. Bearpark, J. J. Heyd, E. Brothers, K. N. Kudin, V. N. Staroverov, R. Kobayashi, J. Normand, K. Raghavachari, A. Rendell, J. C. Burant, S. S. Iyengar, J. Tomasi, M. Cossi, N. Rega, J. M. Millam, M. Klene, J. E. Knox, J. B. Cross, V. Bakken, C. Adamo, J. Jaramillo, R. Gomperts, R. E. Stratmann, O. Yazyev, A. J. Austin, R. Cammi, C. Pomelli, J. W. Ochterski, R. L. Martin, K. Morokuma, V. G. Zakrzewski, G. A. Voth, P. Salvador, J. J. Dannenberg, S.

- Dapprich, A. D. Daniels, Ö. Farkas, J. B. Foresman, J. V. Ortiz, J. Cioslowski and D. J. Fox, *Gaussian 09, Revision D.01*, Gaussian, Inc., Wallingford, CT, 2009.
- 44 Y. Zhao and D. G. Truhlar, *Theor. Chem. Acc.*, 2008, **120**, 215–241.
- 45 Y. Zhao and D. G. Truhlar, *Acc. Chem. Res.*, 2008, **41**, 157–167.
- 46 A. V. Marenich, C. J. Cramer and D. G. Truhlar, *J. Phys. Chem. B*, 2009, **113**, 6378–6396.
- 47 Y. Yang and P. Liu, *ACS Catal.*, 2015, **5**, 2944–2951.
- 48 Y. Yang, S.-L. Shi, D. Niu, P. Liu and S. L. Buchwald, *Science*, 2015, **349**, 62–66.
- 49 Y. Yang, I. B. Perry, G. Lu, P. Liu and S. L. Buchwald, *Science*, 2016, **353**, 144–150.
- 50 C. Y. Legault, *CYLVIEW, 1.0b*, Université de Sherbrooke, 2009.
- 51 A Hammett study shows that more electron-rich styrene leads to increased reaction rate (see Fig. S4[†]). Our previous study provides an example of promoting CO₂ insertion *via* polarizing CO₂ using a Lewis acid: X. Lv, L. Zhang, B. Sun, Z. Li, Y.-B. Wu and G. Lu, *Catal. Sci. Technol.*, 2017, **7**, 3539–3545.
- 52 C. A. Tolman, *Chem. Rev.*, 1977, **77**, 313–348.
- 53 L. Falivene, R. Credendino, A. Poater, A. Petta, L. Serra, R. Oliva, V. Scarano and L. Cavallo, *Organometallics*, 2016, **35**, 2286–2293, Based on the geometries of (PR₃)Ir(CO)₂Cl and (NHC)Ir(CO)₂Cl optimized using the BP86 functional and a mixed basis set of SDD for Ir and TZVP for other atoms, the % V_{bur} of the monophosphine and NHC ligands were calculated using the web-based SambVca 2.0 program (<https://www.molnac.unisa.it/OMtools/sambvca2.0/index.html>). The default parameters in SambVca 2.0 were used as suggested by Cavallo: sphere radius: 3.5 Å, distance from the center of the sphere: 2.1 Å, mesh spacing: 0.1 Å, H atoms omitted, atom radii: Bondi radii scaled by 1.17.
- 54 D. G. Gusev, *Organometallics*, 2009, **28**, 6458–6461.
- 55 In addition to the suppressing effect of bulkier NHC ligands on the reactivity, the computations show that the reactions with bulkier styrenes, such as α -methylstyrene, *trans*- β -methylstyrene, and mesitylethylene, are also slowed down (see detailed energy profiles in Fig. S5[†]).
- 56 F. M. Bickelhaupt and K. N. Houk, *Angew. Chem., Int. Ed.*, 2017, **56**, 10070–10086.